Direct Dynamics Simulations of Collision- and Surface-Induced Dissociation of N-Protonated Glycine. Shattering Fragmentation†

Samy O. Meroueh, Yanfei Wang, and William L. Hase*

Department of Chemistry and Institute for Scientific Computing, Wayne State University, Detroit, Michigan 48202-3489

Received: March 8, 2002; In Final Form: July 17, 2002

Direct dynamics classical trajectory simulations are used to study energy transfer and unimolecular dissociation in collisions of N-protonated glycine, $(gly\text{-}H)^+$, with an argon atom and a hydrogenated diamond {111} surface. The $(gly\text{-}H)^+$ potential is represented by the AM1 semiempirical electronic structure theory and analytic potentials developed previously are used for the diamond surface and the $(gly\text{-}H)^+$/Ar and $(gly\text{-}H)^+$/diamond intermolecular potentials. The AM1 potential for $(gly\text{-}H)^+$ gives the same collisional energy transfer distributions as does the AMBER empirical force field. For $(gly\text{-}H)^+$ + diamond {111} at a collision energy and angle of 70 eV and 45°, the average percent energy transfer to $(gly\text{-}H)^+$ vibration/rotation, to the surface, and to final ion translation are 12, 38, and 50, respectively. A distribution of $(gly\text{-}H)^+$ dissociation products are observed in these collisions, with ~55% of the dissociations occurring while $(gly\text{-}H)^+$ collides with the surface, i.e., shattering fragmentation. Shattering is initiated when the orientation of $(gly\text{-}H)^+$ and the "hardness" of the collision "drives" a H-atom from CH_2 to the carbonyl carbon or a H-atom from NH_3 to the carbonyl oxygen or ejects a H_2 molecule from NH_3. Shattering is not important in $(gly\text{-}H)^+$ collisions with Ar at 13 eV and an impact parameter of zero, but as found for the surface collisions, the Ar collision may "force" H-atom transfer. The simulations suggest that nonstatistical fragmentation dynamics may be important in the collisional dissociation of protonated amino acids and peptides. The collision may directly "drive" the ion to a fragmentation transition state structure.

I. Introduction

Collision-induced dissociation (CID)[1] and surface induced dissociation (SID)[2,3] are important experimental tools for determining structural properties of ions and energetic and mechanistic information concerning their dissociation pathways. In CID, the ion is energized by a collision with an atom (e.g., Ar) or molecule (e.g., N_2), whereas in SID, the energizing collision is with a surface. If electronic excitation is unimportant, the collision translational energy E_i is partitioned between the final translational energy E_f, the internal vibrational/rotational energy transfer to the ion ΔE_{int}, and energy transfer to the surface ΔE_{surf} or to vibration/rotation of a nonmonotonic gaseous collider:

$$E_i = E_f + \Delta E_{int} + \Delta E_{surf} \quad (1)$$

It is generally thought that the distribution of energy transfer to the ion is narrower in SID than in CID.[4−6] However, a recent study shows that the distribution of internal energy in multiple collision activation CID can be as narrow as internal energy distributions obtained from SID.[7]

Peptide ion fragmentation has been studied by both CID and SID,[7−12] and Jack Beauchamp and co-workers[8] pioneered these CID experiments. Possible peptide ion fragmentation sites are illustrated in Figure 1 for a general tripeptide. At low collision energy (<100 eV), peptides dissociate mainly along their backbone structure forming b_n and y_n ions.[13,14] Further dissociation of the b_n ion into a_n + CO is also commonly observed.[7,9] For these low energy collisions, it has been proposed that the peptide is first activated and then dissociates through a charge directed mechanism.[15−17] Deuterium labeling studies have shown that the proton added to peptides is very mobile and samples various sites with a labile hydrogen before fragmentation occurs.[15−17] Further experimental[11] and theoretical[18] studies have supported the proton mobile model for peptide dissociation. Extensive quantum mechanical calculations along with RRKM modeling were carried out by Csonka et al.[18] to evaluate the mobile proton model. They find that proton-transfer lifetimes are well within the experimental time-scale and conclude that the proton can be considered as labile. The groups along the peptide backbone can act as proton acceptors. A recent study by He et al.[19] finds a correlation between the proton affinity and dissociation threshold. They find that the presence of basic amino acids along a peptide chain tends to inhibit lability of the proton, which increases the reaction threshold. In contrast to charge directed fragmentation at low energies, for high energy collisions, the fragmentation is thought to be prompt and to proceed via a charge remote mechanism.[20,21]

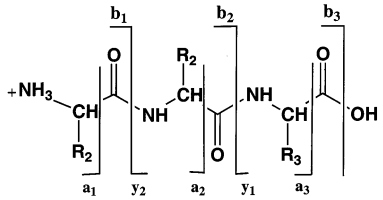

Figure 1. Possible fragmentation sites for a tripeptide.

Initially, studies of peptides were restricted to mapping potential energy surfaces and to structural analysis of neutral

† Part of the special issue "Jack Beauchamp Festschrift".
* To whom correspondence should be addressed.

10.1021/jp020664q CCC: $22.00
Published on Web 08/24/2002

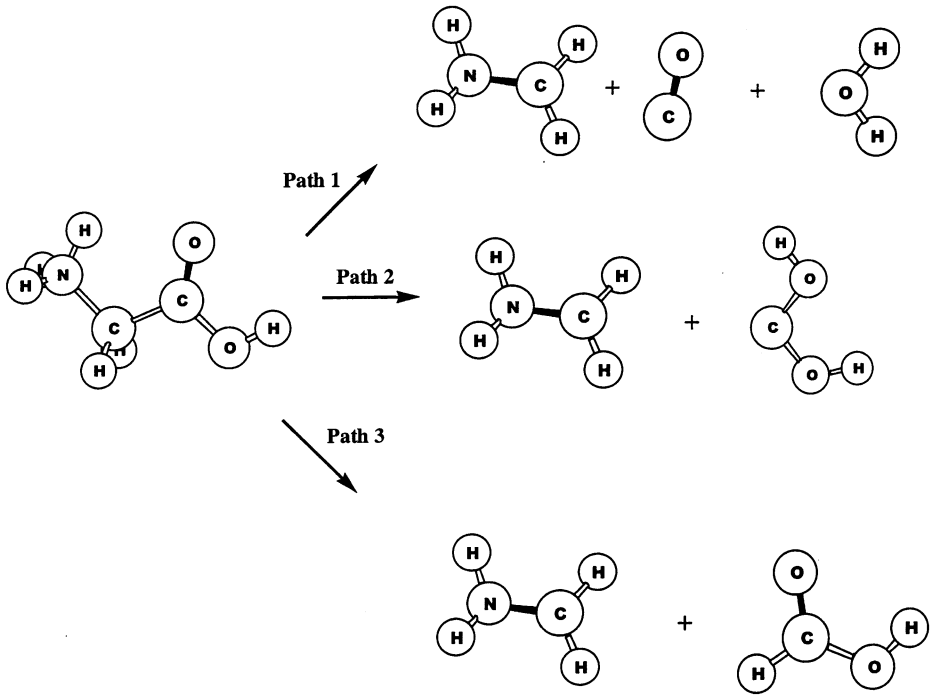

Figure 2. Previously proposed dissociation pathways for N-protonated glycine.

peptides.[22−28] However, with the recent surge of interest in the CID and SID of protonated peptides in the gas phase, these calculations have been extended to protonated amino acids[9,18,29−35] and small peptides.[7,29,36−44] Ab initio calculations have been used to determine proton affinities and basicities of these molecules in the gas phase.[36,38,40] Because peptides in the gas phase can be protonated at any of the backbone amide nitrogens and carbonyl oxygens, these calculations are useful for identifying the site of protonation. Zhang et al.[31,36] have carried out extensive experimental and computational studies of glycine and diglycine. An important finding of their work is that the preferred site for protonation is the amino nitrogen, in agreement with previous theoretical[25] and experimental[9] work. *Ab initio* calculations have also been used extensively to study reaction pathways of small peptides.[9,18,29−44] However, because ab initio calculations of reaction pathways become prohibitive for large molecules, these studies have been confined to amino acids[29,30,33−35] and dipeptides.[39,44]

Glycine is the simplest amino acid. The reaction pathways for its protonated form have been extensively studied both theoretically[9,29−31,33] and experimentally.[9,45,46] Three major fragmentation pathways have been proposed and are shown in Figure 2. The first involves intramolecular proton transfer from the NH_3 group to the OH group, resulting in loss of water and formation of iminium ion ($NH_2CH_2^+$) and CO. For the second pathway, there is proton transfer from the NH_3 group to the carbonyl oxygen, resulting in the loss of dihydroxycarbene, $C(OH)_2$. Formic acid (HCOOH) is formed in the third pathway. The heat of reaction, estimated from thermochemical data,[30,45] is 33, 64, and 26 kcal/mol for paths 1, 2, and 3, respectively.

Path 1, with loss of water and the formation of a b_n ion, was first proposed by Tsang and Harrison.[47] In the case of glycine, b_1 ($NH_2CH_2CO^+$) has never been observed in mass spectra,[47,48] whereas b_n ions where $n > 1$ are frequently observed.[49,50] Recent ab initio calcualtions[32,32,55] have shown that the decomposition of b_1 into a_1 and CO is exothermic, and thus, b_1 is not expected to be detected in experiments. The b_1 ion is found to be an ion−molecule complex and is more stable than the separate iminium and CO products.[51] Recently, Klassen and Kebarle[9] have carried out CID experiments of small peptides, including glycine, and determined a threshold of 44 kcal/mol for the dissociation of protonated glycine. They considered this threshold as an upper limit and, on the basis of energetics, concluded that path 1 is the most likely dissociation channel. Path 2, formation of the dihydroxycarbene by heterolytic cleavage of the peptide bond, was proposed by Beranova et al.[45] in an extensive study of the reaction pathways of protonated glycine. Recent ab initio calculations show that dihydroxycarbene formation has a barrier of about 60 kcal/mol.[30] Two attempts have been made to detect the presence of neutral dihydroxycarbene.[45,50] In the most recent,[45] neutralization−reionization mass spectrometry (NRMS) was used as a means to try to detect the neutral dihydroxycarbene product, but it was not observed.

Classical trajectory simulations have been used to study the collisional activation of small peptides.[8,52−56] In CID simulations of collisions of the N-protonated peptides polyglycine $(gly)_n$ and polyalanine $(ala)_n$ with Ar[54], up to 75% of the collision energy is transferred to peptide internal energy, and visualization of individual trajectories shows substantial deformation of the activated peptide, which may facilitate intramolecular proton transfer.[18] Further trajectory studies of the mechanism of energy transfer show that 80% of the collision energy is initially absorbed by low-frequency torsions, which are important for conformational changes of the peptides.[55] Simulations of N-protonated $(gly)_3$ and $(gly)_5$ SID, by collisions with *n*-hexylthiolate self-assembled monolayer (SAM) and diamond {111} surfaces, show that energy transfer to the peptide is more efficient for collision with the hard diamond surface than the soft SAM surface.[56] These simulations also show that 80% of the initial energy transfer to the peptide is to its torsions, in agreement with the CID simulations. In peptide activation by SID, the percent energy transfer to the peptide is nearly independent of E_i for collision with the SAM but is nonmonotonic and peaking at E_i of about 30 eV for collision with diamond.

All previous molecular dynamics simulations of the collisional activation of peptides have been carried out on a harmonic potential energy surface, which does not allow peptide

TABLE 1: Enthalpy Barriers for (gly-H)$^+$ Dissociation[a]

products	B3LYP[b]	QCISD(T)[c]	MP2[b]	AM1[d]
$NH_2CH_2^+ + CO + H_2O$	41.4(74.6)	35.6(75.4)	38.5(79.0)	40.3(65.4)
$NH_2CH_2^+ + C(OH)_2$	57.2(69.8)	51.5(61.7)	63.1(75.7)	27.2(40.5)
$NH_2CH_2^+ + HCOOH$	88.5	85.0	92.9	99.5
$NH_3CH_3^+ + CO_2$	74.0	78.4	77.5	78.2
$NH_2CHCOOH^+ + H_2$	80.0[e]			86.8

[a] The barriers are for 300 K. The ab initio calculations are from ref 30, except for the last reaction. The barriers in parentheses are those for the higher energy mechanisms discussed in the text. [b] Calculations with 6-31G* basis. [c] Calculations with 6-31+G** basis. [d] This work. [e] Calculations with the 6-31++G** basis from ref 29.

fragmentation.[8,52−56] In the work presented here, direct dynamics classical trajectory simulations are reported of CID and SID of N-protonated glycine, (gly-H)$^+$. The potential energy and gradients for (gly-H)$^+$ are determined "on the fly" directly from electronic structure theory using the AM1 semiempirical electronic structure model.[57,58] In the CID and SID simulations, (gly-H)$^+$ collides with an Ar atom and a diamond {111} surface, respectively. Reaction pathways are characterized for fragmentation of (gly-H)$^+$, and each trajectory is visualized to study the atomic-level dynamics of fragmentation. The energy transfer probabilities obtained using the AM1 potential for (gly-H)$^+$ are compared with those determined using the AMBER force-field[59] for (gly-H)$^+$. It is important to determine how the simulation results depend on the model used for the (gly-H)$^+$ intramolecular potential.

II. AM1 Energetics and Mechanisms

For the work presented here, the AM1 semiempirical potential model is used to represent the (gly-H)$^+$ intramolecular potential. To examine the accuracy of this model, it is important to compare its reaction pathways and energetics with those determined previously from experiment[9] and ab initio calculations.[29,30] In the following, the AM1 mechanisms and energetics for the previously proposed reaction paths in Figure 2 are described. AM1 and ab intio barriers are also compared for additional (gly-H)$^+$ fragmentation pathways. Both the AM1 and ab initio barriers are listed in Table 1.

The AM1 microscopic mechanisms for paths 1, 2, and 3 in Figure 2 were determined by locating stationary points along their reaction paths. Two different mechanisms were found for path 1, yielding the iminium ion $CH_2NH_2^+$, H_2O, and CO. For one, there is first H-atom transfer from the hydroxyl to the carbonyl group, followed by proton migration from the amino group. The resulting moiety first undergoes loss of water and then CO. According to ab initio calculations,[30] the proton-transfer step corresponds to the highest activation enthalpy, with a value of 35.6−41.4 kcal/mol (Table 1). The AM1 calculations give the same rate determining step, with a similar activation enthalpy of 40.3 kcal/mol. Furthermore, the ab initio and AM1 activation enthalpies agree with the experimentally determined[9] upper limit of 44.4 kcal/mol.

For the second mechanism, proton transfer from the amino group occurs first, followed by a second proton migration, with subsequent fragmentation to the reaction products. The AM1 barrier for this mechanism is 65.4 kcal/mol and significantly higher than that for the first. The rate controlling transition states for both mechanisms are shown in Figure 3.

Two mechanisms are also found from the AM1 calculations for path 2 in Figure 2. For the first, proton migration to the carbonyl group is followed by breaking of the peptide bond to yield the iminium ion and dihydroxycarbene. The proton-transfer

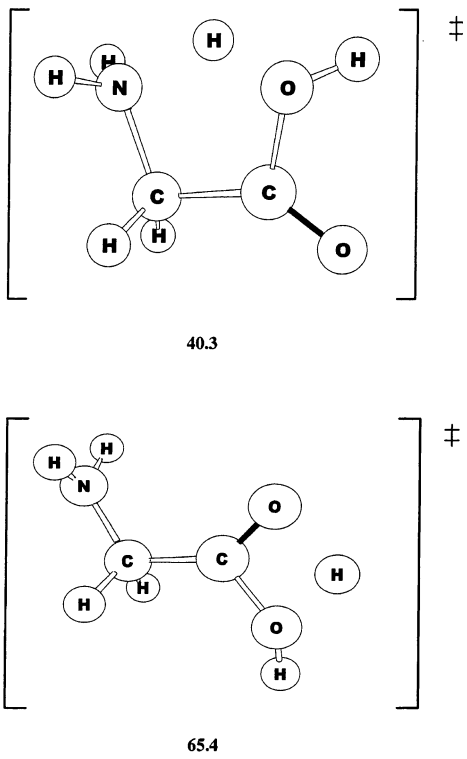

Figure 3. Structures of the AM1 rate-controlling TSs for mechanisms 1 and 2 for path 1 in Figure 2. The enthalpies of the TSs are with respect to (gly-H)$^+$.

step has the highest activation barrier of 27.2 kcal/mol, whereas decomposition to yield dihydroxycarbene has a 20.0 kcal/mol barrier. In contrast, ab initio calculations[30] find that peptide bond fission to yield dihydroxycarbene has the largest activation barrier of 51−63 kcal/mol, substantially larger than the AM1 value. For the second mechanism, rotation of the hydroxyl group is followed by proton transfer and then breaking of the peptide bond with an overall 30.5 kcal/mol barrier. In agreement with the ab initio calculations,[30] the highest AM1 barrier corresponds to the loss of dihydroxycarbene. However, the AM1 activation enthalpy of 30.5 kcal/mol is substantially smaller than the ab initio values in Table 1. The rate controlling transition states for both mechanisms are shown in Figure 4.

Formation of formic acid from protonated glycine dissociation, path 3 in Figure 2, was first proposed by Meot-Ner[60] and more recently by Zhang et al.,[22] both from CID experiments. It was suggested[30] that formic acid forms via a four-centered transition state, where a proton migrates from the amino group to the carbonyl carbon, followed by C−C bond rupture. Previous ab initio calculations give a reaction barrier of 85−93 kcal/mol. The AM1 calculation gives the same mechanism (see Figure 5) and a barrier of 99.5 kcal/mol and only slightly larger than the ab initio values.

The AM1 reaction pathways for CO_2 and H_2 formation are shown in Figure 6. The barrier for CO_2 is 78.2 kcal/mol and in good agreement with the ab initio values in Table 1. H_2 is formed when a H atom of the amino group reacts with a H atom of the CH_2 group. The AM1 barrier for this reaction is 86.8 kcal/mol and only slightly higher than the 80.0 kcal/mol B3LYP/6-31++G** value.[29]

A summary of the AM1 and ab initio barriers for the above (gly-H)$^+$ decomposition reactions is given in Table 1. Except for the $C(OH)_2$ formation channel, the AM1 and ab initio barriers are in agreement.

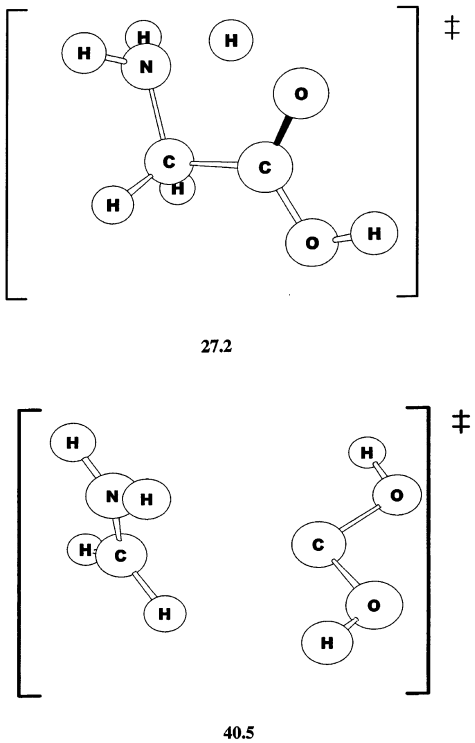

Figure 4. Structures of the AM1 rate-controlling TSs for mechanisms 1 and 2 for path 2 in Figure 2. The enthalpies of the TSs are with respect to $(gly\text{-}H)^+$.

III. Potential Energy Function

The general potential energy function used for the $(gly\text{-}H)^+$/Ar and $(gly\text{-}H)^+$/diamond {111} systems is given by

$$V = V_{peptide} + V_{surface} + V_{peptide,surface} \quad (2)$$

where $V_{peptide}$ is the $(gly\text{-}H)^+$ intramolecular potential, $V_{surface}$ is the potential for the diamond surface, and $V_{peptide,surface}$ represents either the $(gly\text{-}H)^+$/diamond or $(gly\text{-}H)^+$/Ar intermolecular potential. As described above, the AM1 semiempirical electronic structure theory model[57,58] is used for the $(gly\text{-}H)^+$ intramolecular potential. The remaining potentials are analytic functions, described in detail previously.[54,56,61] The potential energy function for the diamond {111} model consists of harmonic stretches and bends, with force constants chosen to fit the diamond phonon spectrum.[61] The $(gly\text{-}H)^+$/diamond and $(gly\text{-}H)^+$/Ar intermolecular potentials are modeled by a sum of two-body potentials between the atoms of the peptide and Ar and the atoms of diamond. The two-body potential is given by

$$V_{XY} = A_{XY}\exp(-B_{XY}r_{ij}) + \frac{C_{XY}}{r_{ij}^6} \quad (3)$$

where X corresponds to Ar or the C and H atoms of the diamond and Y corresponds to H, C, O, and N atoms of the peptide. To determine the parameters for the two-body potentials, ab initio potential energy curves were calculated[54,56] using CH_4 as a model for the C and H atoms of the diamond {111} and CH_4, NH_3, NH_4^+, H_2CO, and H_2O as models for the different types of atoms and functional groups comprising peptides. The ab initio calculations were carried out at the MP2/6-311+G(2df,2pd) level of theory with the frozen-core approximation.[54,56]

IV. Computational Procedure

The classical trajectory[62−64] simulations were carried out with the general chemical dynamics package VENUS[65] interfaced with the semiempirical electronic structure theory computer program MOPAC.[66] Initial conditions for the trajectories were chosen to model experiments. The $(gly\text{-}H)^+ + Ar$ collisions were restricted to an impact parameter $b = 0$. As described previously,[54,56] $(gly\text{-}H)^+$ was randomly rotated about its center-of-mass to sample all collision orientations. To simulate the $(gly\text{-}H)^+ +$ diamond collisions, the center of a beam of $(gly\text{-}H)^+$

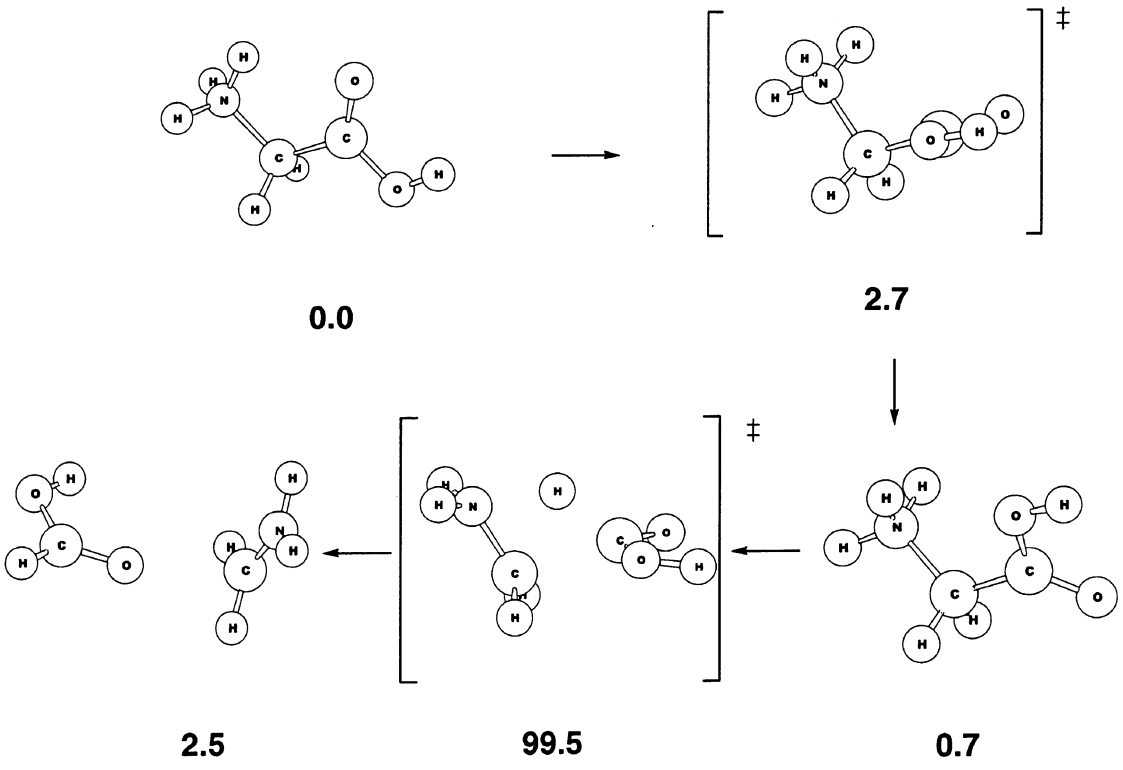

Figure 5. AM1 mechanism for path 3 in Figure 2. The enthalpies are with respect to $(gly\text{-}H)^+$.

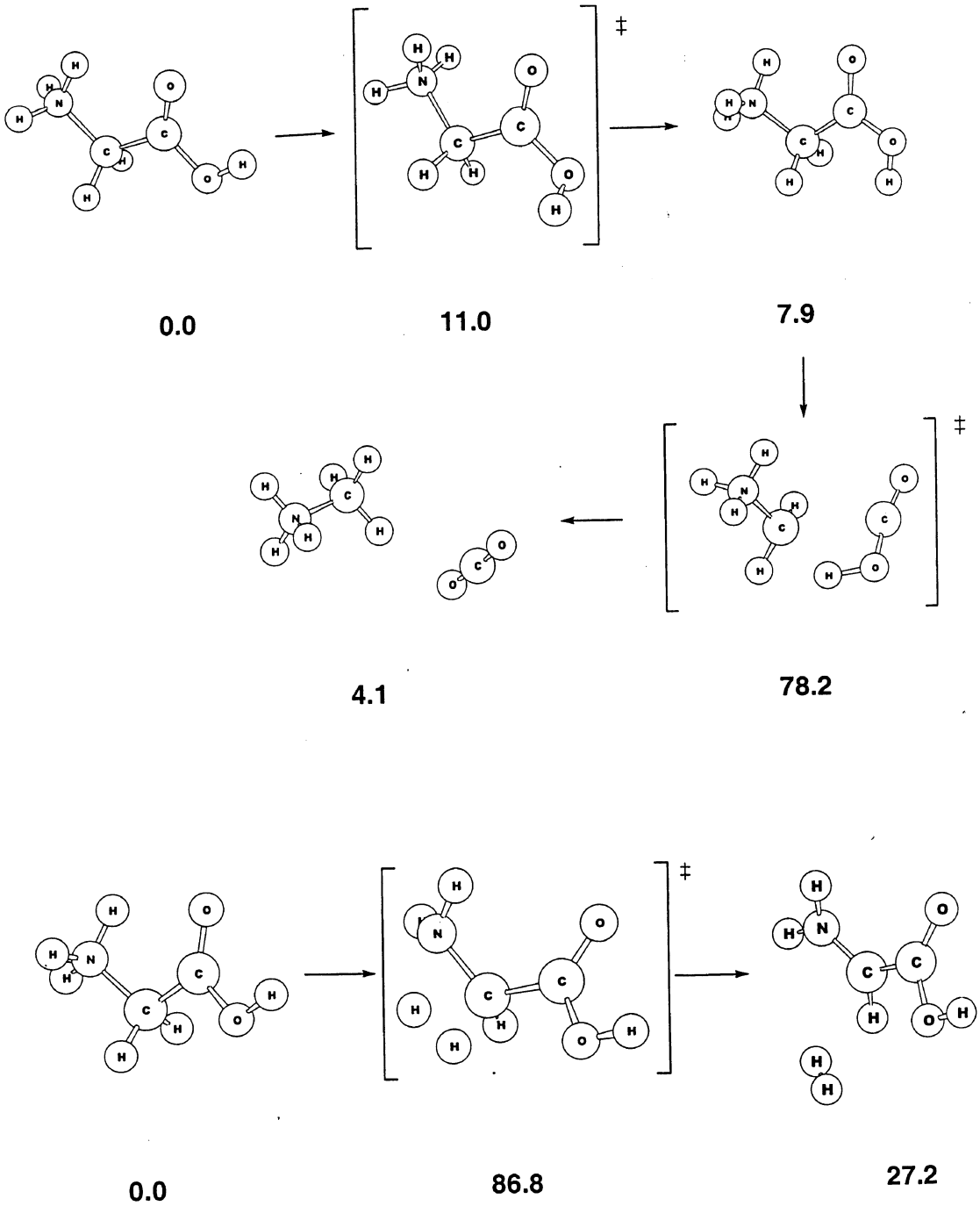

Figure 6. AM1 reaction pathways for CO_2 and H_2 formation.

ion projectiles is aimed at the center of the surface, with fixed incident angle θ_i and fixed initial translational energy, E_i. The radius of the beam was chosen so that the beam overlapped a unit area on the surface, and the trajectory results are insensitive to its radius. Following the procedure described previously,[67,68] the projectile for each trajectory was randomly placed in the cross-section of this beam and randomly rotated about its center-of-mass so that it has an initial random orientation with respect to the surface. The azimuthal angle, χ, between the beam and a fixed plane perpendicular to the surface was sampled randomly between 0 and 2π. Such a random sampling of χ simulates collisions with different domains of growth on the diamond surface.[68] The distance between the center of the beam and the center of the top of the surface was set to 30 Å.

The initial conditions for the vibrational modes of the $(gly\text{-}H)^+$ were chosen via the quasiclassical normal mode method,[64,69−71] which includes zero-point energies. Excess energies, for each normal mode of vibration, were selected from the mode's 300 K harmonic oscillator Boltzmann distribution.[71] The energy was randomly partitioned between kinetic and potential by choosing a random phase for each normal mode.[69] A 300 K rotational energy of RT/2 was added to each principal axis of rotation of the projectile.

Initial conditions for the diamond surface were chosen by assigning velocities sampled from a Maxwell−Boltzmann distribution at 300 K to the surface atoms. The surfaces were then equilibrated for 2 ps of molecular dynamics by scaling the velocities[72] so the temperature corresponds to that for a 300 K classical Boltzmann distribution. The structure obtained from this equilibration process is then used as the initial structure for a 0.1 ps equilibration run at the beginning of each trajectory. A time step of 0.1 fs was used to integrate the classical

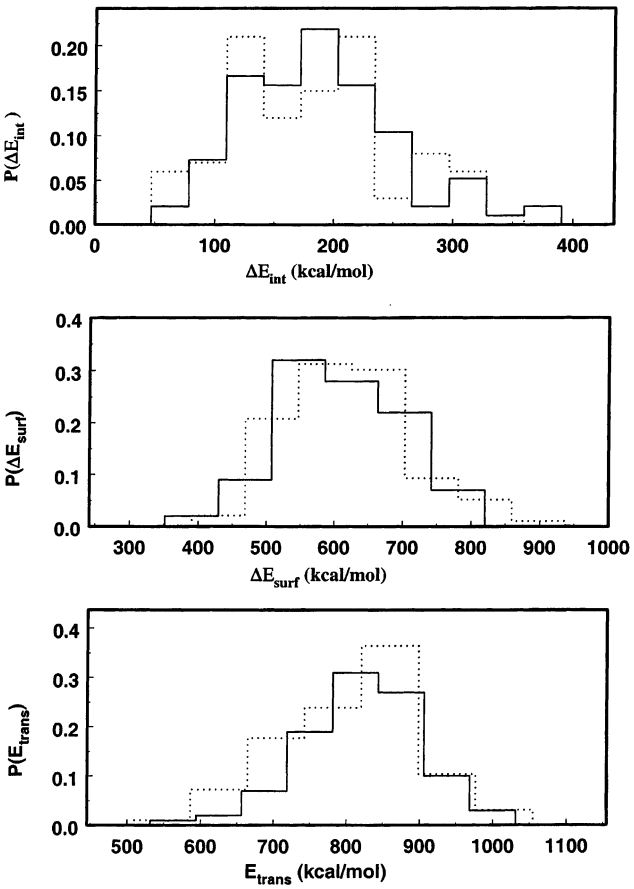

Figure 7. Distributions of the energy transfer to $(gly\text{-}H)^+$ vibration/rotation ($E_i \rightarrow E_{int}$), the surface ($E_i \rightarrow E_{surf}$), and translation ($E_i \rightarrow E_{trans}$) for the $(gly\text{-}H)^+$ intramolecular potential represented by the AMBER force field (—) and AM1 (....). Results for $(gly\text{-}H)^+$ colliding with diamond {111} at an initial energy and angle of 70 eV and 45°.

equations of motion, to ensure conservation of energy to 8 significant figures.

A total of 100 trajectories were computed for both the $(gly\text{-}H)^+ + Ar$ and $(gly\text{-}H)^+ +$ diamond simulations. For the former, $E_i = 13$ eV and $b = 0$. For the latter, E_i and θ_i are 70 eV and 45°. When the trajectory is terminated, the projectile's internal energy change ΔE_{int} is determined by subtracting the initial value of the projectile's internal energy from its final value. The energy transferred to the surface ΔE_{surf} is then determined from the energy conservation relationship in eq 1. Each trajectory was animated to investigate the energy transfer and fragmentation dynamics.

V. Trajectory Results

A. Energy Transfer Distributions. Comparison of AMBER and AM1 Potentials for $(gly\text{-}H)^+$. For $(gly\text{-}H)^+$ collisions with Ar, at an impact parameter $b = 0$ and initial relative translational energy E_i of 13 eV (300 kcal/mol), 45% of E_i is transferred to $(gly\text{-}H)^+$ vibrational/rotational energy E_{int} for both the AMBER and AM1 intramolecular potential models for $(gly\text{-}H)^+$. Similar agreement between the AMBER and AM1 energy transfer probabilities is found for collisions of $(gly\text{-}H)^+$ with the diamond {111} surface at E_i of 70 eV (1614 kcal/mol) and collision angle of 45°. For the AMBER potential, the percents of energy transfer to E_{int}, E_{surf}, and E_f are 11, 37, and 52, respectively. Using the AM1 potential, these percents are nearly identical, i.e., 12, 38, and 50. Figure 7 shows that the AMBER and AM1 potentials give very similar energy transfer distributions for $(gly\text{-}H)^+$ colliding with diamond {111}. A similar type of agreement is found between the energy transfer distributions for the $(gly\text{-}H)^+ + Ar$ collisions. The calculations presented here show that, to simulate energy transfer in $(gly\text{-}H)^+$ CID and SID, the harmonic AMBER and anharmonic reactive AM1 potentials give the same result.

B. Dynamics of $(gly\text{-}H)^+ + Ar$ CID. A total of 100 trajectories were calculated to simulate $(gly\text{-}H)^+$ colliding with an Ar atom at $E_i = 13$ eV (300 kcal/mol) and $b = 0$ Å. The trajectories were integrated for 4.0 ps and during this time 32 of the energized $(gly\text{-}H)^+$ ions fragmented. Four trajectories followed path 1 in Figure 2, 11 followed path 2, and two followed path 3. An additional trajectory formed formic acid, as in path 3, but gave the NH_3CH^+ ion instead of iminium $NH_2\text{-}CH_2^+$. Thus, 19 of the 32 reactive trajectories, i.e., ~60%, followed the three previously proposed paths in Figure 2. However, a substantial number of additional dissociation pathways are observed. Though some of the fragmentation occurred within a short time of the inner turning point in the $Ar + (gly\text{-}H)^+$ relative motion, none occurred during the collision, which would be considered shattering fragmentation.

1. $NH_2CH_2^+ + H_2O + CO$ Products. Each of the four dissociations forming the $NH_2CH_2^+ + H_2O + CO$ products is initiated when a proton from the amino group migrates to the hydroxyl group. The dissociations are illustrated in Figure 8, where the distances between the transferring hydrogen and the hydroxyl oxygen, the carbonyl carbon and hydroxyl oxygen, and the two carbon atoms are plotted versus time. For the trajectory on the upper left side of the figure, the $Ar + (gly\text{-}H)^+$ collision occurs at 160 fs, and proton migration and shortening of the O—H distance occurs 235 fs later at 395 fs, with a concomitant increase in the C—O distance and formation of the b_1 ion and H_2O. The b_1 ion is not long-lived, and loss of CO follows H_2O formation by about 100 fs.

The proton-transfer time is defined here as the time elapsed between the time between the inner turning point in the $Ar + (gly\text{-}H)^+$ relative motion and the time the distance between the transferring H atom and hydroxyl O atom becomes less that 1.2 Å. The resulting proton-transfer times for the four trajectories are 80, 235, 580, and 2910 fs. Proton migration from NH_3 to the hydroxyl group is not instantaneous and may require a picosecond or more. Similarly, the lifetimes for the b_1 ion are 133, 191, 206, and 231 fs. These short times are consistent with previous ab initio and experimental studies,[32,34,50] which have found that the b_1 ion undergoes facile CO loss and is a transient species.

2. $NH_2CH_2^+ + C(OH)_2$ Products. A total of 11 trajectories form the dihydroxycarbene product. The reaction occurs when a proton migrates from the amino group to the carbonyl oxygen, followed by rupture of the C—C bond forming $NH_2CH_2^+$ and $C(OH)_2$. Proton-transfer times for the trajectories, determined as above, are −5, −5, +7, +9, +270, +454, +724, +1293, +3037, +3644, and +3667 fs. Four of the proton transfers occur nearly instantaneously, and of these, two take place before the inner turning point in the $Ar + (gly\text{-}H)^+$ relative motion. Animations of these trajectories show that the argon atom collides "head on" with the NH_3 group of $(gly\text{-}H)^+$ pushing a H atom into the carbonyl oxygen. In this case, hydrogen migration is induced directly by translational energy rather than by $(gly\text{-}H)^+$ internal energy.

For the other trajectories leading to $C(OH)_2$ formation, the times τ for proton transfer are much longer, with the transfer occurring after the $Ar + (gly\text{-}H)^+$ collision. Interestingly, the collisional activation is different for those with τ less than 1000

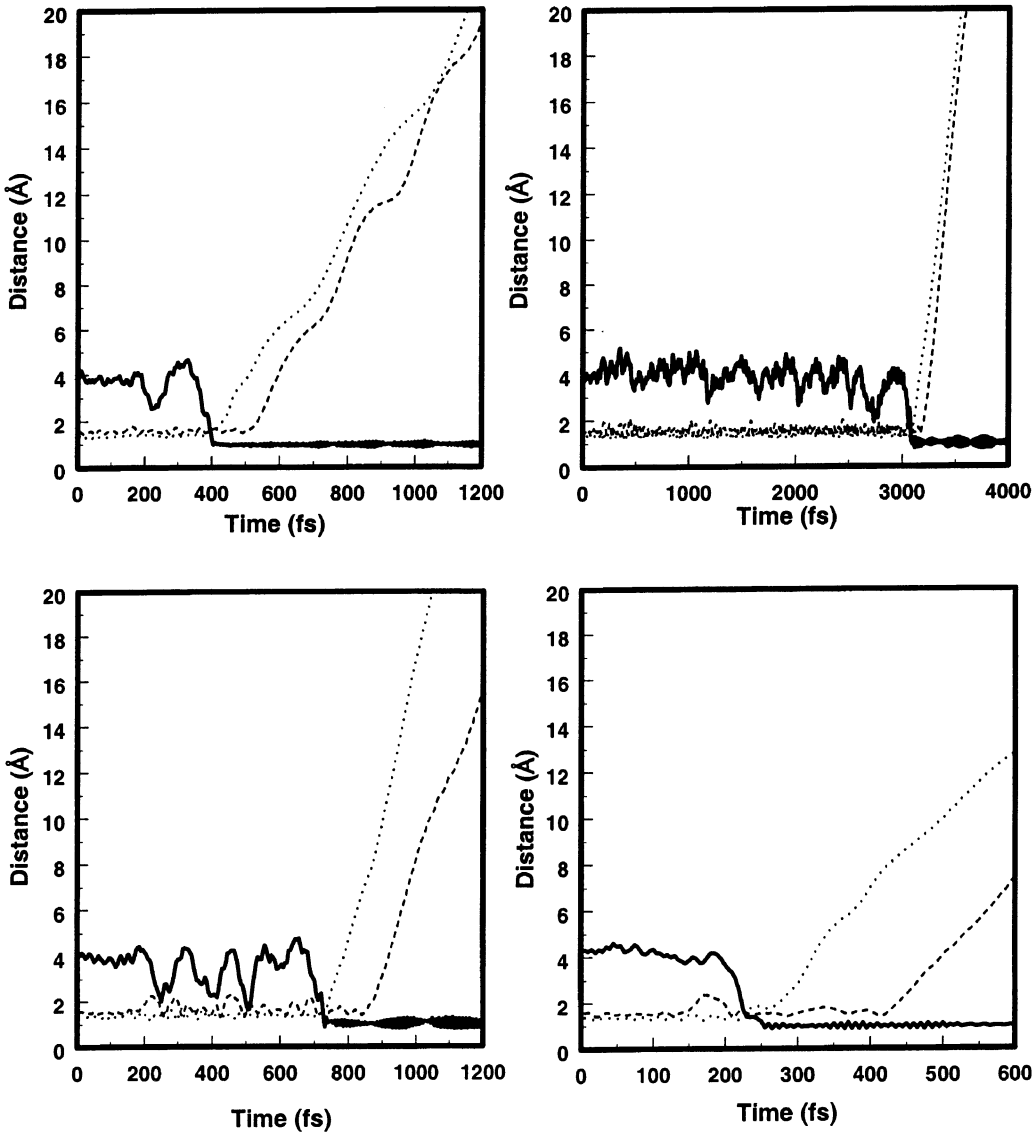

Figure 8. Distances between the transferring H atom and hydroxyl O atom (—), the carbonyl C atom and hydroxyl O atom (....), and the two carbon atoms (— - —) versus time for the four CID trajectories forming $NH_2CH_2^+ + H_2O + CO$.

fs than for those with τ greater than 1000 fs. For τ less than 1000 fs, Ar collides with the "top" of $(gly\text{-}H)^+$, approximately within the NCCO plane, and hitting the CCO unit, where O is the carbonyl oxygen. For τ greater than 1000 fs, the collision is with the "side" of $(gly\text{-}H)^+$ and Ar mainly impacting CH_2 and CO.

It is not surprising that $C(OH)_2$ formation is highly favored given that AM1 underestimates the activation barrier by ~30 kcal/mol. However, the AM1 H-atom transfer barrier is in approximate agreement with the ab initio result,[30] i.e., a barrier of 27.2 and 15.8 kcal/mol at the AM1 and QCISD(T)/6-31+G** levels, respectively. Thus, the H-atom transfer dynamics observed here should be correct and suggest that in experiments H-atom migration from NH_3 to C=O should be frequent, leading to the formation of the carbenium ion $NH_2CH_2C(OH)_2^+$. However, subsequent dissociation into $NH_2CH_2^+$ and $C(OH)_2$ may not be highly probable because of its high barrier.

3. $NH_2CH_2^+$ + HCOOH Products. Three trajectories form formic acid. Two follow the mechanism of the AM1 and ab initio calculations (Figure 5), for which H-atom migration from NH_3 to the carbonyl carbon is concomitant with C−C bond rupture to yield $NH_2CH_2^+$ and HCOOH. The remaining trajectory gives HCOOH via H-atom transfer from the CH_2 group to the carbonyl carbon. The initially formed NH_3CH^+ ion later converts to $NH_2CH_2^+$.

4. NH_3 + CO + CH_2OH^+ Products. Ammonia and carbon monoxide were formed from five trajectories by two routes. For one trajectory, CO is ejected upon impact by the argon atom, with association of the OH group and $NH_3CH_2^+$ to form NH_3-CH_2OH^+. This species then dissociates into NH_3 and CH_2OH^+. For the other four trajectories, the NH_3 group first dissociates, and then the hydroxyl group associates with the carbon of CH_2 giving CO and CH_2OH^+. Three trajectories formed NH_3, with no subsequent dissociation of CH_2COOH^+ during the trajectory integration.

5. $NH_3CH_3^+ + CO_2$ Products. Three trajectories formed the products CO_2 and $NH_3CH_3^+$. Each followed the pathway found by the AM1 and ab initio calculations (Figure 6). The OH group rotates so that its H atom may transfer to CH_2. This occurs concurrently with C−C bond rupture, yielding the reaction products.

C. $(gly\text{-}H)^+$ + Diamond {111} SID. A total of 100 trajectories were calculated to simulate the fragmentation dynamics of $(gly\text{-}H)^+$ energized by collision with the diamond {111} surface at $E_i = 70$ eV and $\theta_i = 45°$. As listed in Table 3, 42 of the $(gly\text{-}H)^+$ ions fragmented, and of the many product channels,

TABLE 2: Products of (gly-H)$^+$ + Ar CID[a]

products	no.	products	no.
no reaction	68	$NH_2CH_2^+ + HCOOH$	2
$NH_3CH_3^+ + CO_2$	3	$NH_2CH_2^+ + H_2O + CO$	4
$NH_3CH_2^+ + COOH$	2	$NH_4^+ + CO + H_2CO$	1
$NH_3CH^+ + HCOOH$	1	$NH_3 + CH_2COOH^+$	3
$NH_2CH_2^+ + C(OH)_2$	11	$NH_3 + CH_2OH^+ + CO$	5

[a] The collision energy is 13 eV, and the impact parameter is zero. Of the 100 trajectories calculated, 32 fragmented to products during the 4.0 ps of the numerical integrations.

TABLE 3: Products of (gly-H)$^+$ + Diamond SID[a]

products	no.[b]	products	no.[b]
no reaction	58	$NCH + 2H_2 + COOH^+$	1(1)
$NH_3CH_3^+ + CO_2$	1	$NCH + H_2 + H_2O + COH^+$	1(1)
$NH_3CH_2^+ + COOH$	3(1)	$NH_3 + CH_2COOH^+$	7(1)
$NH_3CH^+ + HCOOH$	4(4)	$NH_2 + CH_3^+ + CO_2$	1
$NH_2CH_2^+ + C(OH)_2$	7(3)	$NH_3CHCO^+ + H_2O$	1
$NH_2CH_2^+ + HCOOH$	1(1)	$NH_2CHCOOH^+ + H_2$	1(1)
$NH_2CH_2^+ + H_2O + CO$	3	$NH_2CHO + H_2 + COH^+$	1(1)
$NH_2CH_2^+ + H_2 + CO_2$	1(1)	$NCC(OH)_2^+ + 2H_2$	1(1)
$NHCH_2 + H_2 + COOH^+$	6(5)	$NCCHOH^+ + H_2 + H_2O$	1(1)
$NHCH^+ + 2H_2 + CO_2$	1(1)		

[a] The collision energy and angle are 70 eV and 45°. Of the 100 trajectories, each of 1.5 ps, 42 fragmented to products. [b] The number of the fragmentations, which are shattering, are given in parentheses.

the predominant ones are $NH_3CH^+ + HCOOH$, $NH_2CH_2^+ + H_2O + CO$, $NH_2CH_2^+ + C(OH)_2$, $NHCH_2 + H_2 + COOH^+$, and $NH_3 + CH_2COOH^+$. Thus, paths 1 and 2 in Figure 2 are important, and formic acid is also formed, though not by path 3. The iminium ion $NH_2CH_2^+$ is formed in 12 of the trajectories, and its isomer NH_3CH^+ is formed in four. One H_2 or two H_2 molecules are products in 14 of the trajectories, and NH_3 is a product in eight. An important component of the dissociation dynamics is shattering fragmentation, in which (gly-H)$^+$ dissociates as it either impacts or strongly interacts with the surface. A total of 23 of the dissociations, ~55%, occurred by shattering and their dynamics are discussed in more detail below.

1. HCOOH Formation. Formic acid is only formed by shattering. For the four trajectories with NH_3CH^+ as a product, (gly-H)$^+$ is properly oriented as it impacts the surface, so that one of the H atoms of CH_2 is "driven" into the carbonyl C atom, and the products are formed. For the trajectory forming $NH_2CH_2^+$, the above dynamics is the same except $NH_3CH^+ \rightarrow$ H-atom transfer also occurs.

2. H_2 Formation. For H_2 formation, shattering dominates, with 13 of the 14 trajectories dissociating this way via four different mechanisms. For eight of the shattering trajectories, a H_2 molecule is ejected from NH_3 as this end of (gly-H)$^+$ hits the diamond surface. For another three of the shattering trajectories, this H_2 elimination step occurs during the collision, and then later, another H_2 eliminates from CH_2. For the two trajectories forming $NH_2CHCOOH^+$ and $NH_2CHO + COH^+$ as products, the H_2 elimination is four-centered, as proposed previously[29] with one hydrogen coming from nitrogen and the other from carbon. For the one dissociation not occurring by shattering, (gly-H)$^+$ first fragments to $NH_3CH_2^+$ and COOH, and later, the ion dissociates into $NHCH_2^+$ and H_2. Six of the H_2 formation trajectories are plotted in Figure 9.

3. $C(OH)_2$ Formation. Seven of the trajectories form the products $NH_2CH_2^+$ and $C(OH)_2$, three of which occur by shattering. For these seven trajectories, the NH_3 moiety of (gly-H)$^+$ collides with the surface, and six of them transfer a H atom from NH_3 to the carbonyl oxygen during the collision. The

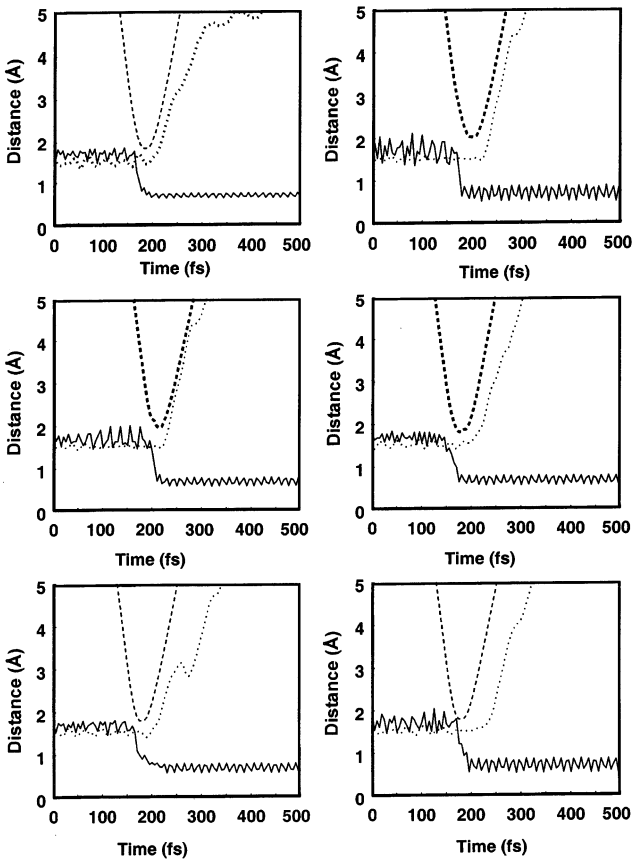

Figure 9. Height of the (gly-H)$^+$ center-of-mass from the top carbon layer of the diamond surface (- - -), the C−C distance (....), and the distance between the eliminating H-atoms (—) versus time for six SID trajectories forming H_2.

distance of the (gly-H)$^+$ center-of-mass from the diamond surface, the C−C distance, and the distance between the transferring H atom and the carbonyl oxygen are plotted in Figure 10 for these six trajectories. Three of the dissociations occur by shattering, for which the C−C bond breaks as the collision promotes transfer of the H atom. For the trajectory not shown in Figure 10, the reaction is nonshattering, and the H atom first transfers to the carbonyl carbon.

4. NH_3 Formation. The product NH_3 is formed in eight, ~ 20%, of the trajectories. For seven, the other product is CH_2COOH^+, whereas for one trajectory, this species undergoes further dissociation to CH_3^+ and CO. For the single shattering trajectory, the N−C bond ruptured on impact. The primary mechanism, for NH_3 formation, is delayed dissociation, with excitation of (gly-H)$^+$ by collision with the surface and then energy accumulation in the N−C bond by intramolecular vibrational energy distribution.[73]

VI. Summary

The following are the important findings from the direct dynamics classical trajectory simulations reported here of the collisions of N-protonated glycine (gly-H)$^+$ with argon atoms at 13 eV and the hydrogenated diamond {111} surface at 70 eV. In the simulations, the intramolecular potential of (gly-H)$^+$ is represented by the AM1 semiempirical electronic structure theory.

1. Using the AM1 potential for (gly-H)$^+$ gives the same average energy transfer values and energy transfer distributions as found when the AMBER empirical force field model is used to represent the (gly-H)$^+$ potential. The AMBER potential gives

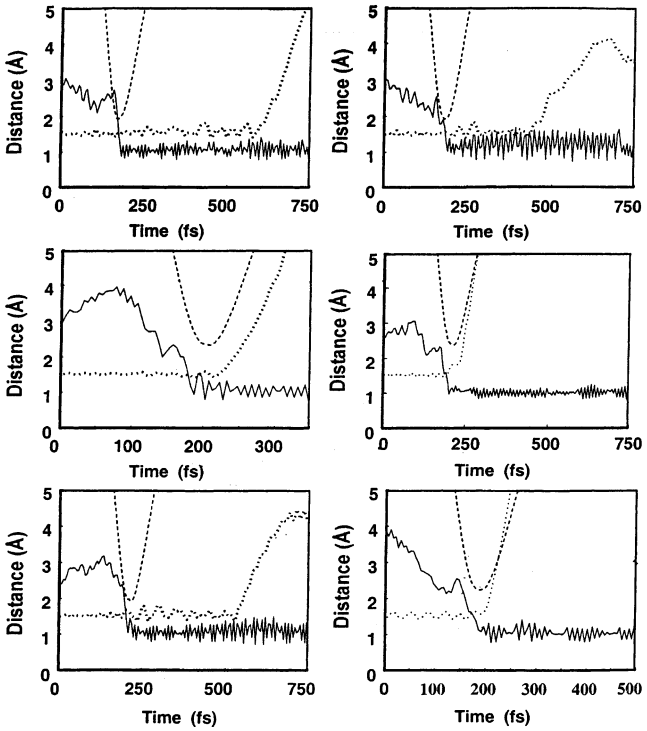

Figure 10. Height of the $(gly\text{-}H)^+$ center-of-mass from the top carbon layer of the diamond surface (- − -), the C−C distance (....), and the distance between the transferring H atom and the carbonyl O atom (—) versus time for the six trajectories which form $NH_2CH_2^+ + C(OH)_2$, by H-atom transfer to the carbonyl O atom. Three of the dissociations occur by shattering.

different anharmonic intramolecular motions for amino acids and peptides than do quantum mechanical potentials.[74] However, this difference does not affect the energy transfer results reported here.

2. For $(gly\text{-}H)^+ + Ar$ collisions, with an intitial energy E_i of 13 eV and impact parameter of zero, 45% of E_i is transferred to $(gly\text{-}H)^+$ vibrational/rotational energy. The transfer of energy, for collisions of $(gly\text{-}H)^+$ with the diamond {111} surface at E_i and θ_i of 70 eV and 45°, is 12% to E_{int}, 38% to the surface E_{surf}, and 50% remaining in translation E_f. From a previous study[56] of $[(gly)_3\text{-}H]^+$ colliding with the diamond surface at the same E_i and θ_i, the percent energy transfers to E_{int}, E_{surf}, and E_f are 17, 21, and 62. The greater percent energy transfer to E_{int} for $[(gly)_3\text{-}H]^+$, as compared to $(gly\text{-}H)^+$, is consistent with the greater number of vibrational modes (particularly torsions)[55] for the former ion. For collisions of $[(gly)_3\text{-}H]^+$ and $[(gly)_5\text{-}H]^+$ colliding with the diamond surface, the energy transfer to the larger peptide is 5 percent units higher.[56] In future studies, it will be important to study collisional energy transfer for more peptides, including those larger and those containing different amino acids.

3. For the $(gly\text{-}H)^+ + Ar$ trajectories, integrated for 4.0 ps, the two principal product channels are $NH_2CH_2^+ + C(OH)_2$ and NH_3 with either CH_2COOH^+ or $CO + CH_2OH^+$ as the other product(s). These two channels constitute 34 and 25% of the $(gly\text{-}H)^+$ dissociations, respectively. The relative amount of the product channel $NH_2CH_2^+ + C(OH)_2$ may be too large, because the AM1 barrier for this channel is too low as compared to the barrier found at higher levels of theory. The previously proposed product channels, $NH_2CH_2^+ + H_2O + CO$ and $NH_2CH_2^+ + HCOOH$ are also observed. An important component of the dissociation dynamics are trajectories that "drive" a NH_3 H atom to the carbonyl oxygen, promoting $NH_2CH_2^+ + C(OH)_2$ formation. This occurs when $(gly\text{-}H)^+$ is properly oriented, as it collides with the hard diamond surface, so that the collision translational energy can directly promote reaction.

4. For the $(gly\text{-}H)^+ +$ diamond {111} trajectories, integrated for 1.5 ps, the three dominant product channels are $NH_2CH_2^+ + C(OH)_2$, $NHCH_2 + H_2 + COOH^+$, and $NH_3 + CH_2COOH^+$. As discussed above, the relative amount of the $NH_2CH_2^+ + C(OH)_2$ product channel may be too large. An important component of the dissociation dynamics for these trajectories is shattering fragmentation, in which $(gly\text{-}H)^+$ dissociates as it either impacts or strongly interacts with the surface. A total of 55% of the dissociations occurred by shattering. Except for one trajectory, all of the formic acid and H_2 are formed by shattering. Formic acid is formed when the collision drives a NH_3 H atom into the carbonyl C atom. Hydrogen formation by shattering occurs when the NH_3 end of $(gly\text{-}H)^+$ hits the surface ejecting H_2 or during the collision H_2 is eliminated by a four-centered reaction, with one hydrogen coming from nitrogen and one from carbon.

The above simulations suggest that the collisional activation of protonated amino acids and peptides may directly "drive" the ion to a dissociation transition state structure, resulting in nonstatistical fragmentation dynamics. To consider the generality of this proposition, in the future, it will be important to study additional amino acids and larger peptides. It is also important to compare the current AM1 direct dynamics with direct dynamics simulations at higher levels of theory, such as B3LYP and MP2. Such work is in progress.

Acknowledgment. The material presented in this manuscript is based upon work supported by the National Science Foundation under Grant No. 0078558. Bill Hase wishes to acknowledge the many enjoyable conversations he has had with Jack Beauchamp concerning ion−molecule and ion chemistry.

References and Notes

(1) Rodgers, M. T.; Armentrout, P. B. *J. Phys. Chem. A* **1997**, *101*, 1238.

(2) (a) Mabud, M. A.; Dekrey, M. J.; Cooks, R. G. *Int. J. Mass Spectrom. Ion Processes* **1985**, *67*, 285. (b) Cooks, R. G.; Ast, T.; Mabud, M. A. *Int. J. Mass Spectrom. Ion Processes* **1990**, *100*, 209.

(3) (a) Kubišta, J.; Dolejšek, Z.; Herman, Z. *Eur. Mass Spectrom* **1998**, *4*, 311. (b) Wörgötter, R.; Kubišta, J.; Zabka, J.; Dolejšek, Z.; Märk, T. D.; Herman, Z. *Int. J. Mass Spectrom Ion Processes* **1998**, *174*, 53.

(4) Vékey, K.; Somogyi, Á.; Wysocki, V. H. *J. Mass. Spectrom.* **1995**, *30*, 212.

(5) Schultz, D. G.; Wainhaus, S. B.; Hanley, L.; de Sainte Claire, P.; Hase, W. L. *J. Chem. Phys.* **1997**, *106*, 10337.

(6) Schultz, D. G.; Hanley, L. *J. Chem. Phys.* **1998**, *109*, 10976.

(7) Laskin, J.; Denisov, E.; Futrell, J. *J. Am. Chem. Soc.* **2000**, *122*, 9703.

(8) Marzluff, E. M.; Beauchamp, J. L. *Large Ions*: *Their Vaporization, Detection and Structural Analysis*; Baer, T., Ng, C. Y., Powis, I., Ed.; John Wiley and Sons Ltd.: New York, 1996; p 115.

(9) Klassen, J. S.; Kerbale, P. J. *J. Am. Chem. Soc.* **1997**, *119*, 6552.

(10) Schultz, D. G.; Lim, H.; Garbis, S.; Hanley, L. *J. Mass Spectrom.* **1999**, *34*, 217.

(11) Dongré, R.; Jones, J. L.; Somogyi, Á.; Wysocki, V. H. *J. Am. Chem. Soc.* **1996**, *118*, 8365.

(12) Laskin, J.; Denisov, E.; Futrell, J. *J. Phys. Chem. B* **2001**, *105*, 1895.

(13) Hunt, Y.; Yates, J. R., III.; Shabanowitz, J.; Winston, S.; Hauer, C. R. *Proc. Natl. Acad. Sci. U. S. A.* **1986**, *83*, 6233.

(14) Yost, R. A.; Boyd, R. K. *Methods in Enzymology*; McCloskey, Ed.; Academic Press: San Diego, CA, 1990; Vol. 193, p 154.

(15) Harrison, G.; Yalcin, T. *Int. J. Mass Spectrom. Ion Processes* **1997**, *165*, 339.

(16) Mueller, D. R.; Eckersley, M.; Richter, W. *Org. Mass Spectrom.* **1988**, *23*, 217.

(17) Johnson, R. S.; Krylov, D.; Walsh, K. A. *J. Mass Spectrom.* **1995**, *30*, 386.

(18) Csonka, I. P.; Paizs, B.; Lendvay, G.; Suhai, S. *Rapid Commun. Mass Spectrom.* **2000**, *14*, 417.
(19) He, F.; Ramirez, J.; Lebrilla, C. *J. Am. Chem. Soc.* **1999**, *121*, 4726.
(20) Ballard, K. D.; Gaskell, S. J. *Int. J. Mass Spectrom. Ion Processes* **1991**, *111*, 173.
(21) Johnson, R. S.; Martin, S. A.; Biemann, K.; Stults, J. T.; Watson, J. T. *Int. J. Mass Spectrom. Ion Processes* **1988**, *86*, 137.
(22) Bohm, H.-J. *J. Am. Chem. Soc.* **1993**, *115*, 6152−6258.
(23) Bohm, H.-J.; Brode, S. *J. Am. Chem. Soc.* **1991**, *113*, 7129−7135.
(24) Cornell, W. D.; Caldwell, J. W.; Kollman, P. A. *J. Chim. Phys. PCB* **1997**, *94*, 1417−1435.
(25) Gordon, M. S.; Jensen, J. H. *J. Am. Chem. Soc.* **1991**, *113*, 7917−7924.
(26) Gould, I. R.; Kollman, P. A. *J. Phys. Chem.* **1992**, *96*, 9255−9258.
(27) Gould, I. R.; Cornell, W. D.; Hillier, I. H. *J. Am. Chem. Soc.* **1994**, *116*, 9250−9256.
(28) Head-Gordon, T.; Head-Gordon, M.; Frisch, M. J.; Brooks, C. L., III.; Pople, J. A. *J. Am. Chem. Soc.* **1991**, *113*, 5989−5997.
(29) Balta, B.; Basma, M.; Aviyente, V.; Zhu, C.; Lifshitz, C. *Int. J. Mass Spectrom.* **2000**, *201*, 69−85.
(30) O'Hair, R. A. J.; Broughton, P. S.; Styles, M. L.; Frink, B. T.; Hadad, C. M. *J. Am. Mass. Soc. Spectrom.* **2000**, *11*, 687−696.
(31) Zhang, K.; Chung-Phillips *J. Chem. Inf. Comput. Sci.* **1999**, *39*, 382−395.
(32) Morpurgo, S.; Bossa, M.; Morpurgo, G. O. *Theochem* **1998**, *429*, 71.
(33) O'Hair, R. A. J.; Reid, G. E. *Rapid Commun. Mass Spectrom.* **2000**, *14*, 1220−1225.
(34) Rogalewicz, F.; Hoppilliard, Y.; Ohanessian, G. *Int. J. Mass. Spectrom.* **2000**, *195/196*, 565−590.
(35) van Dongen, W. D.; Heerma, W.; Haverkamp, J.; de Koster, C. G. *Rapid Commun. Mass Spectrom.* **1996**, *10*, 1237.
(36) Zhang, K.; Zimmerman, D. M.; Chung-Phillips, A.; Cassady, C. J. *J. Am. Chem. Soc.* **1993**, *115*, 10812.
(37) Gömöry, Á.; Vékey, K. *Rapid Commun. Mass Spectrom.* **1996**, *10*, 1485−1496.
(38) Zhang, K.; Cassady, C. J.; Chung-Phillips, A. *J. Am. Chem. Soc.* **1994**, *116*, 11512−11521.
(39) Harrison, A. G.; Csizmadia, I. G.; Tang, T.-H. *J. Am. Soc. Mass Spectrom.* **2000**, *11*, 427−436.
(40) Jiangyue, W.; Lebrilla, C. B. *J. Am. Chem. Soc.* **1993**, *115*, 3270.
(41) Wu, J.; Gard, E.; Bregar, J.; Green, M. K.; Lebrilla, C. B. *J. Am. Chem. Soc.* **1995**, *117*, 9900−9905.
(42) Wu, J.; Lebrilla, C. B. *J. Am. Soc. Mass Spectrom.* **1995**, *6*, 91.
(43) Wu, J.; Gard, E.; Bregar, J.; Green, M. K.; Carlito, B. L. *J. Am. Chem. Soc.* **1995**, *117*, 9900−9905.
(44) Zhu, C.; Balta, B.; Aviyente, V.; Lifshitz, C. *J. Phys. Chem. A* **2000**, *104*, 7061.
(45) Beranovà, S.; Cai, J.; Wesdemiotis, C. *J. Am. Chem. Soc.* **1995**, *117*, 9492.
(46) McCormack, A. L.; Somogyi, À.; Dongré, A. R.; Wysocki, V. H. *Anal. Chem.* **1993**, *65*, 2859.
(47) Tsang, C. W.; Harrison, A. G. *J. Am. Chem. Soc.* **1976**, *98*, 1301.
(48) Cordero, M. M.; Houser, J. J.; Wesdemiotis, C. *Anal. Chem.* **1993**, *65*, 1594.
(49) van Setten, D.; Kulik, W.; Heerma, W. *Biomed. Environ. Mass Spectrom.* **1990**, *21*, 451.
(50) Kulik, W.; Heerma, W. *Biol. Mass Spectrom.* **1991**, *20*, 553.
(51) Rodriquez, C. F.; Vuckovic, D. L.; Milburn, R. K.; Hopkinson, A. C. *J. Mol. Struct.* **1997**, *401*, 117.
(52) Marzluff, E. M.; Campbell, S.; Rodgers, M. T.; Beauchamp, J. L. *J. Am. Chem. Soc.* **1994**, *116*, 7787.
(53) Gilbert, R. G.; Sheil, M. M.; Derrick, P. J. *Org. Mass. Spectrom.* **1985**, *120*, 430.
(54) Meroueh, O.; Hase, W. L. *J. Phys. Chem. A* **1999**, *103*, 3981.
(55) Meroueh, O.; Hase, W. L. *Int. J. Mass Spectrom.* **2000**, *201*, 233.
(56) Meroueh, O.; Hase, W. L. *J. Am. Chem. Soc.* **2002**, *124*,1524.
(57) Dewar, M. J. S.; Zoebisch, E. G.; Healy, E. F.; Stewart, J. J. P. *J. Am. Chem. Soc.* **1985**, *107*, 3902.
(58) Stewart, J. J. P. *J. Comput. Chem.* **1989**, *10*, 209.
(59) Cornell, W. D.; Cieplak, P.; Bayley, C. I.; Gould, I. R.; Merz, K. M.; Ferguson, D. M.; Spellmeyer, D. C.; Fox, T.; Caldwell, J. W.; Kollman, P. A. *J. Am. Chem. Soc.* **1995**, *117*.
(60) Meot-Ner, M.; Field, F. H. *J. Am. Chem. Soc.* **1973**, *95*, 7207.
(61) Hass, K. C.; Tamor, M. A.; Anthony, T. R.; Banholzer, W. F. *Phys. Rev. B* **1992**, *45*, 7171.
(62) Bunker, D. L. *Methods Comput. Phys.* **1971**, *10*, 287.
(63) Bunker, D. L. *Acc. Chem. Res.* **1974**, *7*, 195.
(64) Peslherbe, G. H.; Wang, H.; Hase, W. L. In *Advances in Chemical Physics*; Ferguson, D., Siepmann, J. I., Truhlar, D. G., Ed.; Wiley: New York, 1999; Vol. 105, p 171.
(65) Hase, W. L.; Duchovic, R. J.; Hu, X.; Komornicki, A.; Lim, K. F.; Lu, D.-h.; Peslherbe, G. H.; Swamy, N.; Vande Linde, S. R.; Varandas, A.; Wang, H.; Wolf, R. J. *QCPE* **1996**, *16*, 671.
(66) Stewart, J. J. P. *QCPE* **1989**, *XX*, 451.
(67) Bosio, S. B. M.; Hase, W. L. *Int. J. Mass Spectrom.* **1998**, *174*, 1.
(68) Bosio, S. M.; Hase, W. L. *J. Chem. Phys.* **1997**, *107*, 9677.
(69) Chapman, S.; Bunker, D. L. *J. Chem. Phys.* **1975**, *62*, 2890.
(70) Sloane, C. S.; Hase, W. L. *J. Chem. Phys.* **1977**, *66*, 1523.
(71) Cho, Y. J.; Vande Linde, S. R.; Zhu, L.; Hase, W. L. *J. Chem. Phys.* **1992**, *85*, 958.
(72) Allen, M. P.; Tildesley, D. J. *Computer Simulation of Liquids*; Oxford University Press, Inc.: New York, 1987.
(73) Baer, T.; Hase, W. L. *Unimolecular Reaction Dynamics. Experiments and Theory*; Oxford: New York, 1996.
(74) Wei, D.; Guo, H.; Salahub, D. R. *Phys. Rev. Lett.* **2001**, *64*, 11907.